Cerebral Cortex October 2014;24:2707–2720
doi:10.1093/cercor/bht128
Advance Access publication May 19, 2013

The Structure of Pairwise Correlation in Mouse Primary Visual Cortex Reveals Functional Organization in the Absence of an Orientation Map

Daniel J. Denman and Diego Contreras

Department of Neuroscience, University of Pennsylvania Perelman School of Medicine, Philadelphia, PA, USA

Address correspondence to D. Contreras, Department of Neuroscience, University of Pennsylvania Perelman School of Medicine, 215 Stemmler Hall, Philadelphia, PA 19106-6074, USA. Email: diegoc@mail.med.upenn.edu

Neural responses to sensory stimuli are not independent. Pairwise correlation can reduce coding efficiency, occur independent of stimulus representation, or serve as an additional channel of information, depending on the timescale of correlation and the method of decoding. Any role for correlation depends on its magnitude and structure. In sensory areas with maps, like the orientation map in primary visual cortex (V1), correlation is strongly related to the underlying functional architecture, but it is unclear whether this correlation structure is an essential feature of the system or arises from the arrangement of cells in the map. We assessed the relationship between functional architecture and pairwise correlation by measuring both synchrony and correlated spike count variability in mouse V1, which lacks an orientation map. We observed significant pairwise synchrony, which was organized by distance and relative orientation preference between cells. We also observed nonzero correlated variability in both the anesthetized (0.16) and awake states (0.18). Our results indicate that the structure of pairwise correlation is maintained in the absence of an underlying anatomical organization and may be an organizing principle of the mammalian visual system preserved by nonrandom connectivity within local networks.

Keywords: connectivity, population coding, rodent, synchrony, V1

Introduction

Throughout sensory systems, neurons are organized by response preference, so that like-responding neurons are close to each other, creating a functional map [e.g., orientation pinwheels in primary visual cortex (V1)]. Despite the ubiquity of maps, their role is unclear. For example, although rodent V1 lacks an orientation map (Ohki et al. 2005), single-cell orientation selectivity is not grossly different than in species with an orientation architecture (Niell and Stryker 2008; Gao et al. 2010). In addition, correlations of spike output within a population of responding neurons are also organized by the underlying functional architecture. In V1, pairwise correlated activity depends on the pair's relative orientation preference (Kohn and Smith 2005; Smith and Kohn 2008), relative distance (Kruger and Aiple 1988; Gawne et al. 1991; Smith and Kohn 2008), and among distant cells it is only observed between cells with similar orientation preference (Ts'o et al. 1986).

Correlations reflect the functional connectivity within a network (Perkel et al. 1967). In addition, correlations can affect representation of information by a network in diverse ways, including influencing pooling (Zohary et al. 1994; Abbott and Dayan 1999; Romo et al. 2003) and enhancing postsynaptic integration (Reid and Alonso 1996; Cardin et al. 2010). Any role for these correlations in sensory coding depends on the magnitude of correlation and the structure of correlation relative to space and stimulus parameters (Abbott and Dayan 1999; Deneve et al. 1999; Pouget et al. 1999). In the presence of an orientation map, nearby neighbors often share selectivity for space and orientation, making the local structure of pairwise correlation difficult to determine.

To elucidate the local structure of pairwise correlation in V1, we utilize layer 2/3 of mouse V1, where distance between a pair of cells is independent of relative orientation selectivity. The structure of functional connectivity could reflect disordered functional architecture with random connectivity (Jia et al. 2010; Hofer et al. 2011; Hansel and van Vreeswijk 2012). However, we hypothesized that synaptic specificity of inputs to (Yoshimura et al. 2005) and within (Ko et al. 2011) layer 2/3 networks would result in a structure of pairwise correlations between neurons that is dependent on orientation and distance even in the absence of functional architecture.

We measured pairwise correlation on two timescales: a longer timescale of mean spike count on a trial-to-trial basis (r_{sc}) and a short timescale of synchrony within tens of milliseconds. We found that pairwise synchrony is dependent on the distance and the difference in orientation preference between the cells in each pair. Both visually evoked and spontaneous r_{sc} are also organized by pair distance and orientation preference. Our results show that, in mouse V1, specific synaptic connectivity maintains the structure of pairwise correlation despite the absence of a map.

Materials and Methods

Animal Preparation and Surgery

All procedures were done within the guidelines of the National Institutes of Health and were approved by the University of Pennsylvania Institutional Animal Care and Use Committee. Adult C57/B6 mice (8–24 weeks) were initially sedated with a mixture of xylazine (10 mg/kg) and fentanyl (10 µg/kg); anesthesia was induced with a high concentration of isoflurane (5%) and maintained with continuous inhaled isoflurane (0.1–1%). Additional doses of fentanyl (5 µg/kg) were administered every approximately 2 h to maintain anesthetic plane. The depth of anesthesia was monitored by heart rate (maintained between 300 and 600 beats/min), pupil dilation, pinch reflex, and following the opening of the craniotomy by the level of synchronous activity in the local field potential (LFP). After placement in a stereotactic apparatus, eye moisture was maintained by application of a transparent lubricant and body temperature was maintained at 37°C by rectal monitoring and a heating pad (FHC Inc., Bowdoin, ME, USA). A 2-by-2 mm craniotomy was opened over V1. To minimize damage during electrode penetration, the dura was resected across the majority of the craniotomy using a dura hook and the exposed surface was coated with a layer of silicon oil. Following surgery, the entire stereotactic apparatus was rotated 60° to position the contralateral eye in front of the display screen.

For separate set of animals ($n = 3$), a survival surgery was performed at least 1 week prior to a single recording session. During this surgery, two fixation bolts were permanently implanted and a V1 craniotomy was performed. The exposed V1 was covered with silicon oil and the

opening resealed. On the day of recording, the mouse was head-fixed on a passive treadmill using the implanted bolts. The temporary seal over V1 was removed, mouse rotated 60° to position the contralateral eye, and tetrodes lowered as described above. The mouse was allowed to run freely and transitioned between passive and active behavioral states.

Electrophysiology

Following surgery, an array of four to six tetrodes (Thomas Recording GmbH, Giessen, Germany) arranged either linearly or concentrically was inserted into V1 perpendicularly relative to the cortical surface. In both configurations, the tip-to-tip space between neighboring tetrodes was 254 µm. Individual tetrodes were 100 µm in diameter with a central contact at the tip approximately 40 µm below three concentrically arranged contacts around the shaft approximately 20 µm from each other. Signals were preamplified by the tetrode drive and amplified, individually filtered, and acquired at 30 kHz using a Cheetah 32 acquisition system (Neuralynx, Boseman, MT, USA). High-frequency spiking activity was isolated at each contact by filtering between 600 and 6000 Hz. A single channel from each tetrode was duplicated and filtered 0.1–375 Hz to record an LFP. Each tetrode was individually inserted to an initial depth of 100–160 µm. Following a rest period of at least 30 min, each tetrode was lowered through the cortex in 2-µm steps until at least one strong unit was present; in this dataset, all tetrodes were stopped before reaching approximately 350 µm below the cortical surface, the putative boundary of layers 3 and 4.

Visual Stimuli

All visual stimuli were generated using the ViSaGe stimulus generation hardware (Cambridge Research Systems, Cambridge, UK) and a custom software package utilizing the accompanying MATLAB (Mathworks, Natick, MA, USA) toolbox. Stimuli were displayed on a 19-in cathode ray tube monitor configured to refresh at 100 Hz. This monitor was gamma-corrected using a luminometer and ViSaGe configuration software and placed 30 cm from the eye contralateral to the craniotomy. Full-screen stimuli covered approximately 70° of visual field. After tetrode insertion, the screen was set to a background of 50% luminance. Stimuli consisted of drifting sinusoidal gratings. To drive responses from as many cells as possible, all stimuli were 100% contrast and 0.04–0.06 cycles/°, in line with previous reports in mouse visual cortex (Niell and Stryker 2008; Gao et al. 2010; Niell and Stryker 2010). The 70° stimuli were sufficiently large, as the visual space recorded by our most distantly spaced electrodes is approximately 30°; given the median size of a mouse V1 receptive field (Gao et al. 2010) of all cell pairs recorded up to 500 µm are at least partially overlapping (Bonin et al. 2011).

Spike Clustering and Data Analysis

Spike waveforms from each tetrode were clustered into individual units offline using a mixture of algorithmic and manual sorting (SpikeSort3D, Neuralynx). Waveforms were initially sorted using KlustaKwik and subsequently manually refined (e.g., Fig. 1*A*,*B*). All clusters with spikes in the 0–1-ms bin of the interspike interval histogram were strictly rejected. To assess the quality of separation of the identified single units, we measured isolation distance and the L-ratio for each cluster (Fig. 1*C*), which indicate the distance of the center of the cluster from the noise and the quality of the moat around the cluster, respectively (Schmitzer-Torbert et al. 2005). An example set of clustered data in Figure 1*A*–*C* shows the isolation of 6 single units from one tetrode, with isolation distances >10 and L-ratios <0.4.

All analysis of single-cell and pairwise spikes was done using Igor Pro 6.0 (Wavemetrics, Lake Oswego, OR, USA) at 1-ms resolution. Orientation tuning was quantified using the average number of spikes over the duration of stimulus presentation. The orientation tuning curves, across the range 0–360°, were fit with the von Mises function (Swindale 1998):

$$f(\theta) = b_0 + b_1 e^{K(\cos(\theta-\mu)-1)} + b_2 e^{K(\cos(\theta-\mu+\pi)-1)},$$

where b_0 is an offset for the baseline firing rate, b_1 and b_2 independently determine the size of each peak, K is the width parameter, and μ the preferred orientation. The maximum value of this fit was used as the cell's preferred orientation, and the half width at half height indicates the bandwidth of orientation selectivity. The difference in preferred orientation ($\Delta\theta$) is the difference between the maxima for a pair of cells. Orientation selectivity index (OSI) was calculated, from raw responses, as the difference between responses at preferred and orthogonal orientations as follows:

$$\mathrm{OSI} = \frac{R_{\mathrm{preferred}} - R_{\mathrm{ortho}}}{R_{\mathrm{preferred}} + R_{\mathrm{ortho}}},$$

where $R_{\mathrm{preferred}}$ is the response at the preferred orientation, as determined by the circular Gaussian fit, and R_{ortho} is the response at the orientation 90° from $R_{\mathrm{preferred}}$. All reported P-values were calculated using the Wilcoxon rank-sum test.

Correlation Measures

Correlation between pairs of cells was measured on two timescales: trial-to-trial variation in spike count (r_{sc}) and synchrony within 10 ms. Correlated variability was defined as the shared variation, either increase or decrease, in the number of spikes fired over a given time window. The time window used here was the duration of stimulus presentation, which was 2 s. To calculate the r_{sc} for a given pair, the response of each cell was assigned a z-score for each trial:

$$z = \frac{x - \mu}{\sigma},$$

where x is the rate on a given trial, μ the average rate for all trials, and σ the variance. The Pearson correlation was computed as the product of z-scores between a pair summed across all trials:

$$r_{\mathrm{sc}} = \frac{1}{n-1}\sum_{i=1}^{n}\left[\left(\frac{X_i - \overline{X}}{\sigma_X}\right)\left(\frac{Y_i - \overline{Y}}{\sigma_Y}\right)\right],$$

where n is the number of trials, X_i and Y_i the rates for each cell on a given trial, $\overline{X}$ and $\overline{Y}$ the sample means for each cell, and σ_X and σ_Y the sample variance for each cell.

Synchrony was calculated as a peak in a cross-correlogram (CCG) occurring within 10 ms of the zero line. To produce CCGs, we followed Perkel et al. (1967) to compute raw cross correlation; to account for differences in firing across the population, each CCG was divided into the geometric mean of the firing rates of the pair of cells. CCGs were further corrected by the jitter-correction method (Smith and Kohn 2008, Harrison and Geman 2009) using a 50-ms jitter window. Choosing this window size destroys all correlations <50 ms in the correction term, but preserves correlation on all longer timescales. Subtraction of this correction term isolates only the correlation in the raw CCG that occurs on the <50-ms timescale. The presence of a synchronous peak was assessed using a threshold set 2 standard deviations (SD) above the mean level of correlation. Mean correlation was here defined as the mean of the corrected CCG from 100 to 200 ms. The magnitude of synchrony was determined as the area between the threshold and the CCG ±10 ms from the zero line. The correction method used did not affect the presence or the size of synchronous peak (see Fig. 3*C*,*D*). All measurements reported here are based on jitter-corrected CCGs.

To statistically justify the separation of CCG shapes into classes, we measured several parameters from each CCG: width, peak lag, and symmetry. Width was measured at the crossing of the significance threshold. Peak lag was the difference between zero and the time at which the peak occurred. CCG symmetry was measured as follows:

$$\mathrm{symmetry} = \frac{P_0}{P_{max}},$$

where P_0 is the magnitude of the peak at time zero and P_{max} the magnitude of the peak. This measure was taken over ±100 ms, and all values below the significance threshold were treated as baseline (i.e. given a CCG magnitude of zero).

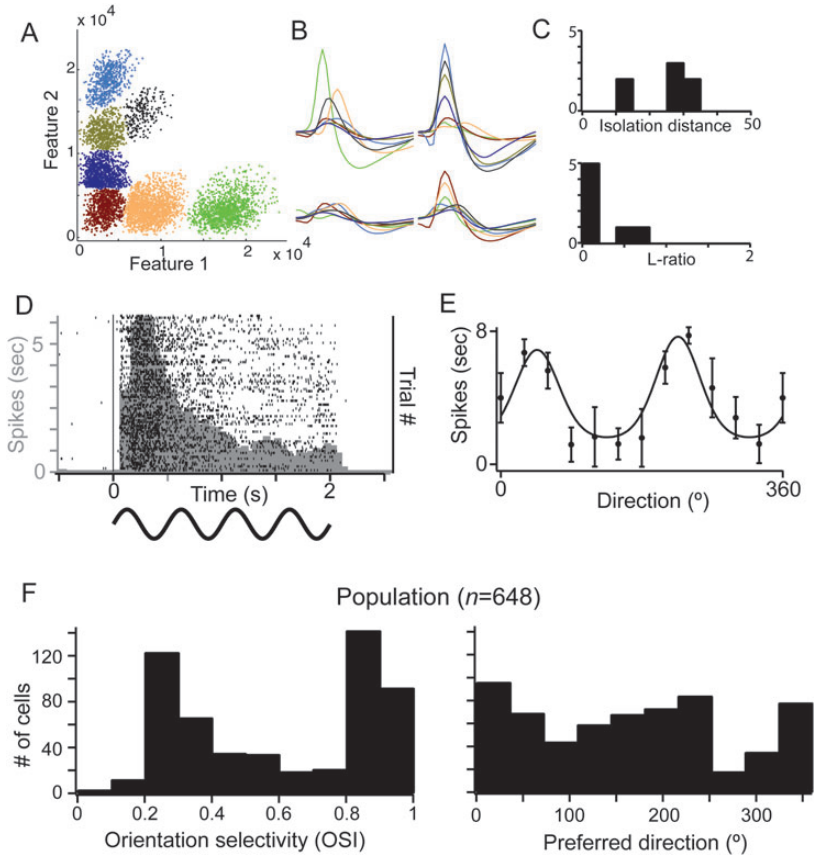

Figure 1. Characterization of simultaneously recorded small population in mouse V1. (*A* and *B*) Example for the separation of spiking activity on a single tetrode into single-cell clusters. (*A*) Spikes from the tetrode, plotted in feature space, and color-coded by cluster assignment. Features 1 and 2 correspond to the waveform peak values on 2 contacts, shown in the top row of *B*. Nonclustered spikes have been removed. (*B*) Average waveform values on each contact for each cluster shown in *A*. (*C*) Spike cluster metrics, isolation distance, and L-ratio, from the example data. (*D* and *E*) Representative response from a single cell in L2/3 of mouse V1. (*D*) Peristimulus time histogram and (*E*) orientation tuning. (*F*) Orientation tuning parameters across the population of recorded neurons. In this and all subsequent figures, error bars are standard error of the mean.

Results

Our goal was to quantify visually driven and spontaneous pairwise correlations of neurons in the supragranular layers 2 and 3 (L2/3) of mouse V1 as a function of their relative distance and their similarity of orientation preference. We recorded single neurons from L2/3 of V1 of anesthetized mice ($n = 38$) using six independently positioned tetrodes. To minimize sampling bias, the position of the tetrodes in L2/3 was not readjusted once a set of cells was detected within the first 370 μm from the pial surface. Individual units were identified using an offline, partially automated clustering procedure (see Materials and Methods; Fig. 1*A*–*C*). Each tetrode sampled up to seven single neurons simultaneously. To maximally drive spiking activity from each population of simultaneously recorded neurons, we used full screen, 100% contrast, drifting sinusoidal gratings optimized in spatial and temporal frequencies for mouse V1 (0.06 cycles/°, 2 Hz; Niell and Stryker 2008; Gao et al. 2010). The example cell in Figure 1*D* responded to repeated presentations of an optimally oriented drifting grating with a nonmodulated increase in the firing rate (mean = 7.2 Hz). The visual response was robust and consistent across trials, as shown by the raster plot (consecutive trials from top to bottom); this cell showed characteristic strong adaptation during the course of the grating as illustrated by the decrease in frequency in the peristimulus time histogram (PSTH, in light gray). Our population consisted almost exclusively of nonmodulating cells with an F_1/F_0 ratio compatible with a classification as complex cells (Supplementary Fig. 1). We plotted the mean firing rate as a function of stimulus orientation ($n = 20$ presentations of each orientation) and used a circular Gaussian fit to generate the orientation tuning curve (Fig. 1*E*). This cell had a preferred orientation of 223° and an OSI of 0.72. We included in our database all cells which fired a minimum of 400 spikes over the 20 min required for the stimulus block, resulting in a total of 648 cells and 4160 simultaneously recorded pairs. Across the population, the mean evoked firing rate was 6.4 ± 7.0 Hz (mean ± SD), spontaneous firing rate was 0.29 ± 0.34 Hz, and the mean half height at half width of orientation tuning curves was 23° ± 8.3°. The OSI distribution was clearly bimodal with a large number of cells highly selective for stimulus orientation (>0.8 OSI) and a large number with weak selectivity (<0.4 OSI). However, there were only 3 untuned cells in our database with OSIs <0.2 (Fig. 1*F*, left panel). The response properties of the cells in our database were consistent with recent quantitative descriptions of mouse V1 (Niell and Stryker 2008; Gao et al. 2010).

Quantification of Correlation

We quantified correlated firing for each pair of simultaneously recorded cells on two timescales, according to previously

established methods (Perkel et al. 1967; Smith and Kohn 2008): (1) synchrony, which measures the pairwise correlation of spike times within ±10 ms, and (2) correlated variability (also called noise correlation, or r_{sc}), which measures the trial-to-trial correlation of spike counts over the duration of each trial (2 s). All measurements of correlation were made from responses to 2 Hz drifting gratings of varying orientation, sufficient to elicit a response from many cells on each trial. Correlations induced by the temporal frequency of these stimuli are broader than the synchrony measured.

We quantified synchrony from the pairwise CCGs (bin = 1 ms) normalized by the geometric mean firing rate and corrected using the subtraction of a 50-ms jitter-correction term to remove stimulus-induced correlation (see Materials and Methods). The "magnitude" of synchrony was the area of the central peak (±10 ms) of the CCG exceeding 2SD above baseline noise (Fig. 2*A*, the dotted line indicates 2SD; see Materials and Methods). The "probability" of synchrony was the ratio of the number of pairs with a significant peak over all recorded pairs. We further subdivided the population of significant CCGs based on the position of the peak with respect to the zero line. A positive peak entirely displaced from the zero line was classified as "offset" synchrony (Fig. 2*A*, left; $n = 90/4160$). This shape is not sufficient to demonstrate a direct connection, but is the most likely explanation for such a shape (Perkel et al. 1967; T'so et al. 1986; Ostojic et al. 2009). A positive peak straddling the zero line was classified as "zero spanning," and is consistent with a shared source of excitatory input (Fig. 2*A*, right; $n = 234/4160$; Perkel et al. 1967). Most zero-spanning peaks were not centered over the zero line (164/234 zero-spanning peaks). The remainder of zero-spanning peaks were centered on zero (70/234). This ad hoc classification of CCGs as offset or zero spanning was supported by the difference in the distribution of peak widths (Fig. 2*B*), showing statistically different means (Fig. 2*E*; $P < 0.005$). The distribution of peak lags, defined as the time of peak relative to zero, was complementary: zero-spanning CCGs were centered on zero (Fig. 2*C*, right), while offset CCGs had a bimodal distribution with centers at 5 and −5 ms (Fig. 2*C*, left). The absolute peak lag was significantly larger for offset CCGs than zero-spanning CCGs (Fig. 2*E*, center; $P < 0.005$). To formalize the difference between the two CCG classes, we measured peak symmetry relative to zero (see Materials and Methods). This value is 1 for peaks exactly centered on the zero line and 0 for peaks fully shifted from the zero line. All offset CCGs showed high asymmetry (Fig. 2*D*, left). Zero-spanning CCGs (Fig. 2*D*, right) had

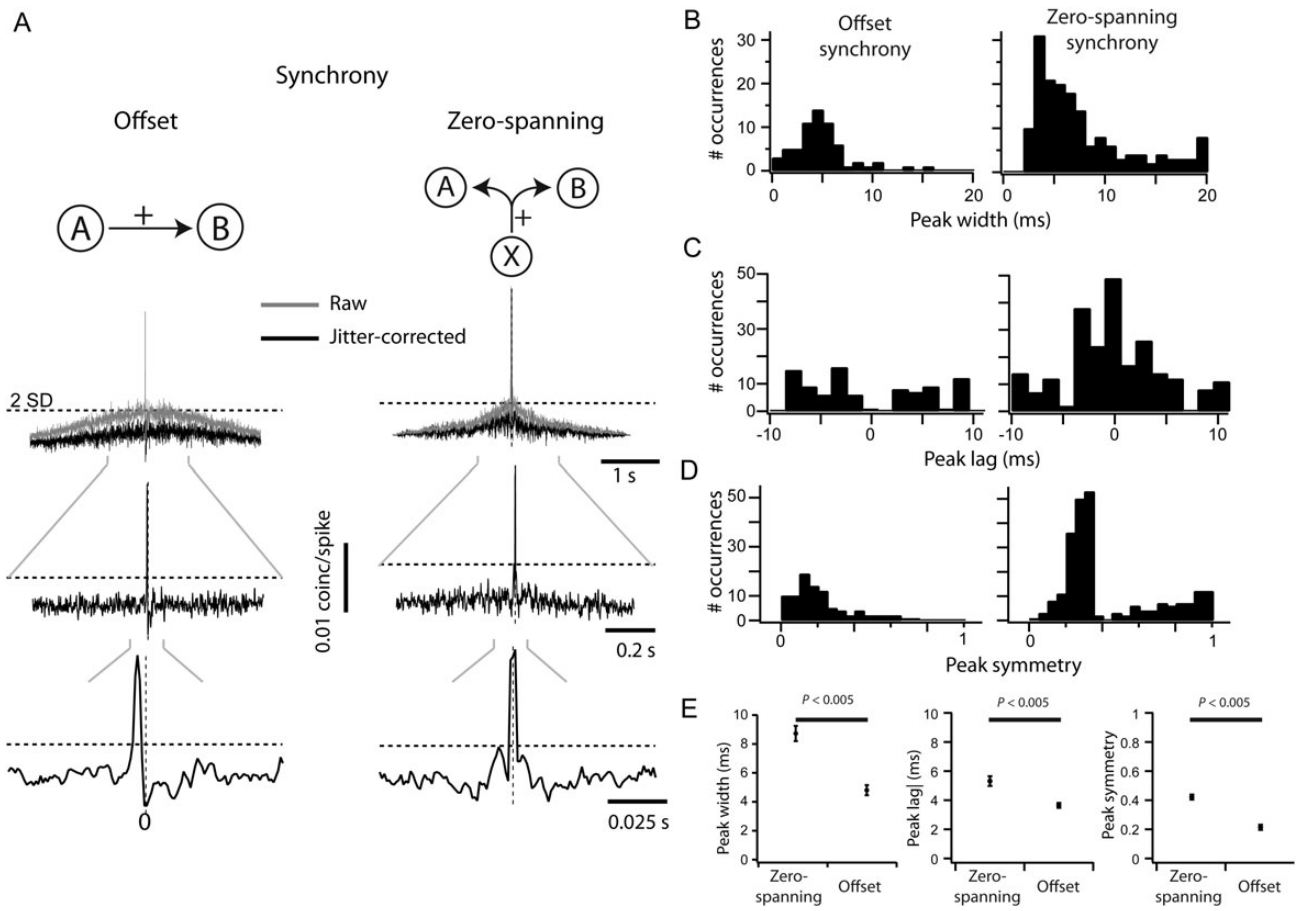

Figure 2. Quantification of pairwise correlation. (*A*) Measuring and classifying synchrony from CCGs. Raw CCGs (gray) were corrected using a 50-ms jitter-correction term. A threshold (dashed lines) was set 2SD above mean in the 100- to 200-ms range of each CCG. Any peak above this threshold within 10 ms of zero was classified as positive; positive peaks were classified as either offset if the entire peak was offset from zero (*A*, left) or zero-spanning otherwise (*A*, right). (*B*) The distributions of peak widths for each CCG class, where peak width is measured at the crossing of the significance threshold. (*C*) The distributions of peak lag for each class of CCG, where peak lag is measured as the time of peak relative to time zero. (*D*) The distributions of peak symmetry for each class of CCG, where peak symmetry is measured as the magnitude of peak at time zero relative to the peak magnitude. (*E*) Comparison of the mean peak width, absolute peak lag, and peak symmetry between CCG classes.

a bimodal distribution of symmetries, with a population of highly symmetrical CCGs (symmetry >0.4; mean: 0.79 ± 0.02) and a population of asymmetrical, yet zero-spanning, CCGs (symmetry <0.4; mean: 0.26 ± 0.005). The subset of symmetrical zero-spanning CCGs was similar to the full population of zero-spanning CCGs in all measurements made subsequently (Supplementary Fig. 2), and so all zero-spanning CCGs were grouped to maximize statistical power.

We tested several factors that could affect measurements of CCG magnitude. We compared the CCG magnitude measured using the jitter-correction method (Smith and Kohn 2008) with two other forms of stimulus correlation removal: shift correction and shuffle correction (Fig. 3*A*,*B*). The method removal of stimulus correlation did not significantly reduce the size of the zero-spanning CCGs or offset CCGs (Fig. 3*B*–*F*). Further, to account for correlations during any onset transient, we removed the first 250 ms of each response after correcting each CCG (Fig. 3*C*,*D*). The removal of this onset transient reduced the peak of some pairs slightly (Fig. 3*D*), but the reduction in CCG magnitude was not significant and smaller than the percentage of spikes removed.

We included pairs recorded on the same tetrode, despite the inability to detect near synchronous spikes for such pairs due to acquisition enforced dead times; because of this, we removed the zero-lag bin from all CCGs from pairs on the same electrode. Peaks from the cells recorded on the same tetrode reflected both forms of synchrony (e.g., Fig. 4*A*). Removing the zero-lag bin affected the classification of CCGs as offset or zero spanning in only 1 of 90 offset CCGs.

We quantified trial-to-trial correlated variability, or r_{sc}, as the Pearson correlation coefficient of standardized mean firing rates across the duration of a trial. This measure is equal to 1 when the covariance between a pair is perfect and 0 when a pair of cells does not covary.

Synchrony as a Function of Orientation Preference

We first examined the dependence of synchrony on the difference in orientation preference, regardless of the distance between neurons in each pair. The difference in orientation preference ($\Delta\theta$, range = 0–90°) was measured as the difference between preferred orientation of the 2 cells in each pair, estimated from the Gaussian fits to the orientation tuning curves (as illustrated in Fig. 1). Figure 4*A* illustrates 3 cells that were isolated on the same tetrode (indicated in black) and therefore, within an approximate radius of approximately 200 µm (Buzsáki et al. 2012). We chose to illustrate a group of cells recorded from the same tetrode to emphasize the fact that neurons in close proximity may show very different orientation preferences (Ohki et al. 2005). Cells 1 and 2 differed only by 18° in their optimal orientation (cell 1: 255° and cell 2: 273°), but diverged by 53° and 35°, respectively, from cell 3 (128°). Cross-correlation revealed zero-spanning synchrony with a magnitude that was dependent on the similarity of orientation preference despite the proximity of the neurons. The strongest synchrony was observed within the pair with the most similar orientation preference (CCG peak = 0.016, cells 1 and 2), while the pair with largest difference in orientation preference showed no significant synchrony (cells 1 and 3), and the

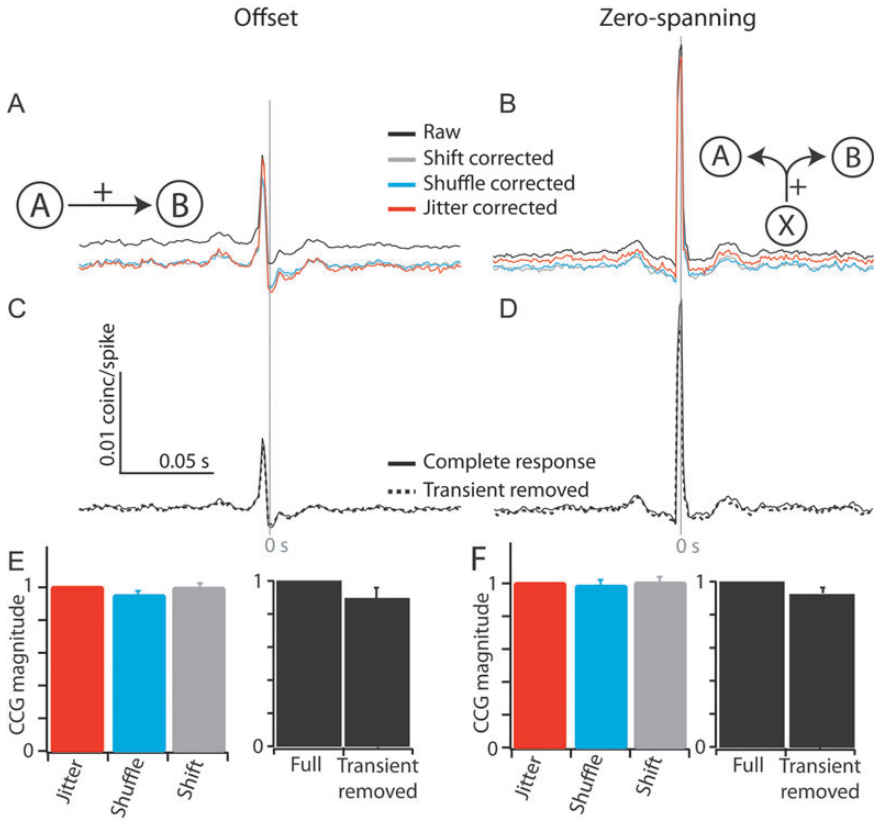

Figure 3. Examination of factors contributing to the measurement of synchrony magnitude. (*A* and *B*) Correction of raw correlograms using 3 correction techniques: Shift (gray line), shuffle (blue line), and jitter (red line), for offset (*A*) and zero-spanning (*B*) CCGs. (*C* and *D*) Removing onset transient did not affect CCG magnitude for offset (*C*) or zero-spanning (*D*) CCGs. (*E* and *F*) Population measures of each factor on CCG magnitude. For the correction method, each CCG is normalized to the magnitude of the jitter-corrected CCG (left). For transient removal, the transient-removed CCG is normalized to the height of the full-response CCG (right).

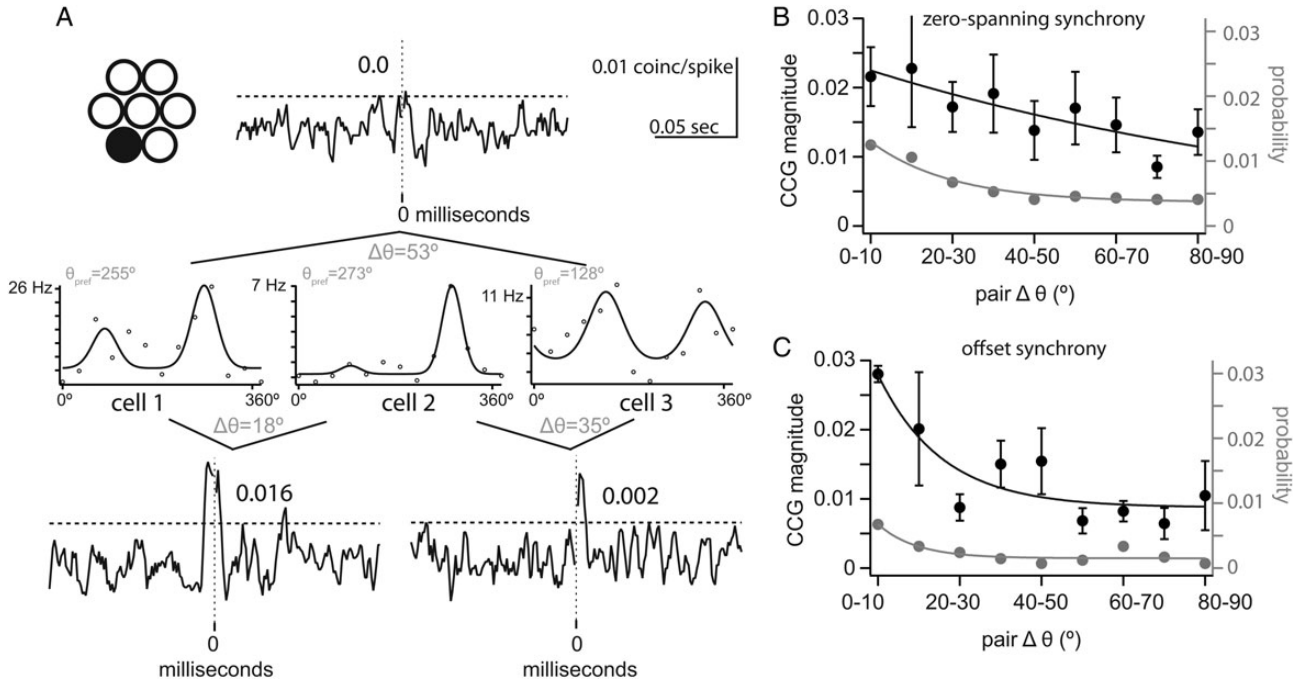

Figure 4. Synchrony is dependent on difference in the orientation preference. (*A*) Example trio of simultaneously recorded pairs. The pair with the most divergent orientation preferences showed no synchrony (top), while the magnitude of synchrony between the remaining pairs was largest for the aligned pair (bottom). (*B*) The magnitude and probability of zero-spanning synchrony depended exponentially on difference in the orientation preference. (*C*) The magnitude and probability of offset synchrony depended exponentially on difference in the orientation preference.

intermediate orientation preference difference showed weaker synchrony (CCG peak = 0.002, cells 2 and 3). This example is inconsistent with the synchrony observed between neighboring neurons at pinwheel singularities in cat visual cortex, where the magnitude of synchrony of nearby neighbors is unaffected by difference in orientation preference (Das and Gilbert 1999).

We obtained population measures of the relationship between synchrony and orientation tuning separately for zero-spanning (Fig. 4*B*) and offset CCGs (Fig. 4*C*). For zero-spanning synchrony, the probability (gray) and magnitude (black) of synchrony were dependent on $\Delta\theta$ and were fit by exponential decay functions ($\chi^2_{prob} = 4 \times 10^{-4}$, $\chi^2_{mag} = 4 \times 10^{-5}$; Fig. 4*B*). The probability of zero-spanning synchrony was higher for cell pairs whose preferred orientations differed by <30° than for cell pairs with less similar orientation tuning (Fig. 4*B*). As a function of $\Delta\theta$, the magnitude of zero-spanning synchrony decreased more slowly ($\tau_{mag} = 126.2°$) than the probability ($\tau_{prob} = 19.9°$; Fig. 4*B*). To determine a criterion $\Delta\theta$ value for magnitude zero-spanning synchrony, we compared each 10° $\Delta\theta$ bin to the first bin (0°–10°); the first significantly different bin was 40–50° ($P = 0.03$), and all subsequent bins were significantly different ($P < 0.05$). We conclude that zero-spanning synchrony is both strongest and most likely within pairs with $\Delta\theta < 40°$, reflecting the specificity of L4 projections to L2/3.

For offset synchrony, probability and magnitude were also dependent on $\Delta\theta$ and were fit by exponential decay functions ($\chi^2_{prob} = 7.5 \times 10^{-5}$, $\chi^2_{mag} = 8.8 \times 10^{-5}$; Fig. 4*C*). The magnitude of offset synchrony decayed similar to probability ($\tau_{mag} = 15.6°$ and $\tau_{prob} = 9.3°$). The probability of offset synchrony was small and relatively flat for $\Delta\theta$ greater than 30° (Fig. 4*C*). The criterion $\Delta\theta$ value for offset synchrony was 10–20° ($P = 0.003$), and all subsequent bins were significantly different ($P < 0.05$); the exponential decay saturated >40°. We conclude that the strength of offset synchrony is strongest within pairs with $\Delta\theta < 40°$, consistent with in vitro measurements of synaptic connections between neighboring cells of known orientation preference (Ko et al. 2011).

The dependence of synchrony on firing rate could affect this measurement (de la Rocha et al. 2007), as dissimilarly tuned cells are less likely to fire spikes on the same trial. However, across $\Delta\theta$, rate-matched pairs yielded exponential fits similar to the full dataset (data not shown), indicating that the effect of stimulus selectivity on synchrony is not dependent on rate.

Synchrony as a Function of Distance

We next considered how the distance between a pair of cells affects synchrony independent of their difference in orientation preference. We found that the distance between a pair of cells, as measured by electrode spacing, significantly affected the probability and magnitude of both types of synchrony. The example in Figure 5*A* shows three neurons recorded from three tetrodes spanning 508 µm. The orientation preference of these cells was very similar, differing by only 4–8° (cell 1: 221°, cell 2: 217°, and cell 3: 225°). Despite the considerable distance between cells 1 and 3, they had a significant zero-spanning CCG peak (magnitude = 0.012). One closer pair had a larger synchrony magnitude in spite of having similar $\Delta\theta$ (cells 1 and 2: 0.026), demonstrating the effect of distance on the magnitude of zero-spanning synchrony, while another closely spaced pair had weaker synchrony (cells 2 and 3: 0.001).

For the population, the decay of probability and magnitude of zero-spanning synchrony as a function of distance were well fit by an exponential decay ($\chi^2_{prob} = 5.7 \times 10^{-3}$,

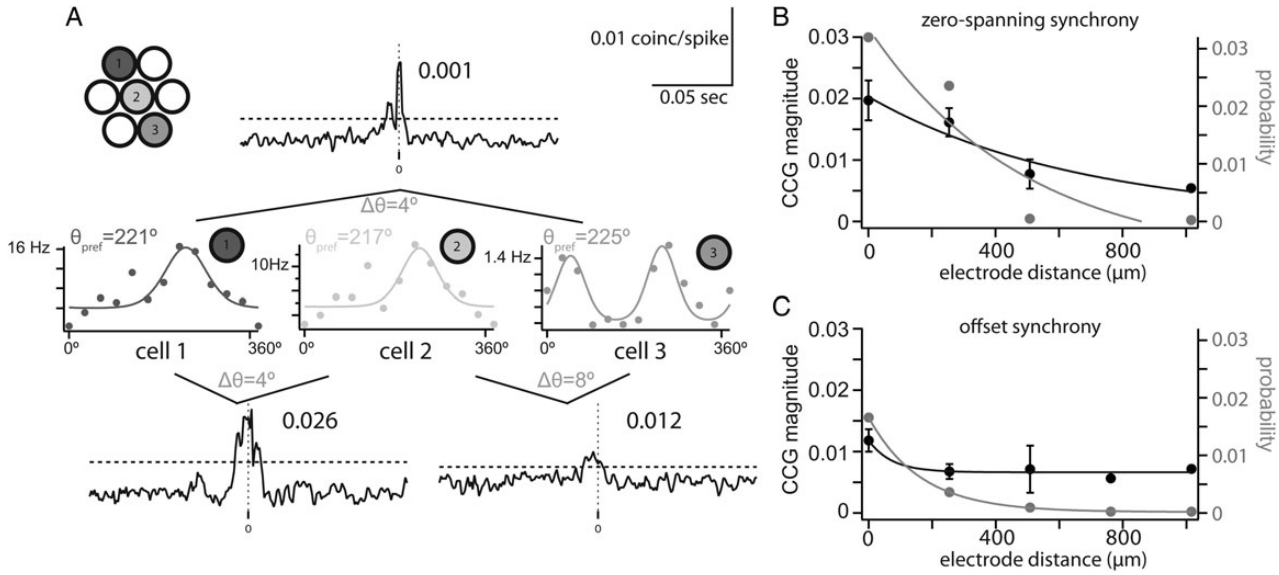

Figure 5. Synchrony is dependent on distance between a pair of cells. (*A*) Example trio of simultaneously recorded pairs. The pair with the largest electrode separation showed weak synchrony (top), while the closer pairs showed stronger synchrony. (*B*) The magnitude and probability of zero-spanning synchrony depended exponentially on pair distance. (*C*) The magnitude and probability of offset synchrony depended exponentially on pair distance.

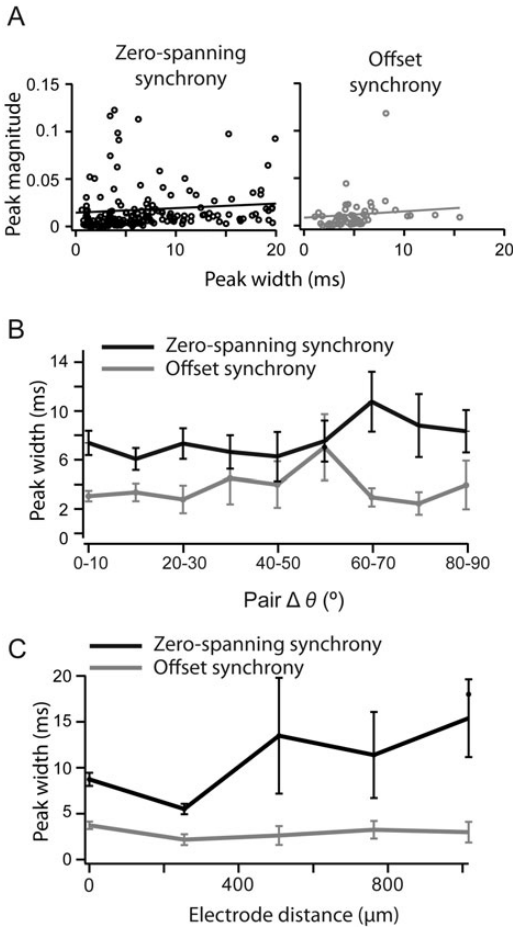

FIgure 6. Offset synchrony width is narrower than zero-spanning synchrony. (*A*) Cross-correlation magnitude measured as a function of peak width for zero-spanning (black, left) and direct synchrony (gray, right). (*B*) Width of CCG peaks, measured at the threshold crossing, as a function of distance between cells for offset (gray trace) and zero-spanning synchrony (black trace). (*C*) The width of CCG peaks as a function difference in preferred orientation for offset (gray trace) and zero-spanning synchrony (black trace).

$\chi^2_{mag} = 1.4 \times 10^{-5}$; Fig. 5*B*). Probability decayed slightly faster than magnitude but on the same order of magnitude ($\tau_{prob} =$ 491.0 μm; $\tau_{mag} = 662.8$ μm). Magnitude dropped significantly at the 508-μm distance (Fig. 5*B*; $P = 0.01$).

The probability of offset synchrony fell exponentially with distance ($\chi^2 = 2.2 \times 10^{-6}$; Fig. 5*C*) much faster ($\tau_{prob} = 162.9$ μm) than zero-spanning synchrony. The magnitude of offset synchrony decayed quickly ($\chi^2_{mag} = 5.4 \times 10^{-6}$, $\tau_{mag} = 72.7$ μm), though the few observations of offset synchrony at distances >508 μm were not significantly smaller than those at smaller distances ($P > 0.05$). Our measurements constrain the spatial extent of the functional networks described by zero-spanning and offset synchrony. The spread of zero-spanning synchrony suggested a wider feedforward network, approximately 1 mm in diameter, compared with a more constrained functional network of offset synchrony, <400 μm in diameter.

Width of Synchrony as a Function of Distance and Orientation Preference

The width of the synchronous peak can affect the measurement of synchrony strength and may be regulated by distinct mechanisms in V1 (Kohn and Smith 2005). Within the allowable window of ±10 ms, we measured the width of the synchronous peak at the point of crossing the 2SD significance threshold. Offset synchrony peaks were significantly narrower (4.8 ± 2.77 ms) than zero-spanning synchrony (8.7 ± 3.29 ms; $P < 0.005$, Wilcoxon rank test, Fig. 2*B*). Narrower offset synchrony peaks are compatible with the underlying hypothesis that this form of synchrony arises from a single source, while zero-spanning peaks can arise from multiple sources. For both types of synchrony peak, peak width was positively correlated with CCG magnitude, though weakly (Fig. 6*A*; slope of the linear fit, zero-spanning: $0.48 \times 10^{-3} \pm 0.28 \times 10^{-3}$; offset: $0.67 \times 10^{-3} \pm 0.45 \times 10^{-3}$). There was no trend in peak width, either offset or zero-spanning, over difference in preferred orientation (Fig. 6*B*). Zero-spanning synchrony was narrower

for nearby cells (<500 μm), even though these nearby pairs had higher synchrony magnitude (Fig. 5*B*), but still not as narrow as offset synchrony (Fig. 6*C*). Across the distances measured, the width of offset synchrony peaks was unchanged (Fig. 6*C*).

Synchrony as a Function of Both Orientation Preference and Distance

Finally, we measured the codependence of both forms of synchrony on distance and $\Delta\theta$, a measurement that is straightforward here because distance and orientation preference are independent across the topography of mouse visual cortex (i.e., there are no orientation pinwheels). Across a network of approximately 1 mm, zero-spanning synchrony is more likely and of larger amplitude for neurons with similar orientation preference (Fig. 7*A–C*). The probability and magnitude of zero-spanning synchrony decreased as a function of distance across all $\Delta\theta$. Notably, probability and magnitude appeared to have the same structure over distance and $\Delta\theta$, reflecting the stimulus specificity of the common input presumably originating in L4 and responsible for the orientation selectivity of L2/3 neurons.

In contrast, the probability of offset synchrony was nearly independent of $\Delta\theta$ for nearby cells (<500 μm; Fig. 7*D*). However, the magnitude of offset synchrony between neighbors was highly dependent on $\Delta\theta$, falling for $\Delta\theta > 20°$. Thus, within smaller networks (<500 μm), connectivity is widespread but the strength of connectivity is $\Delta\theta$ specific. For further separated pairs (>500 μm), the probability of connection was lower and limited to pairs with $\Delta\theta < 30°$; observations of offset synchronous pairs separated by >500 μm and with $\Delta\theta > 30°$ were rare and always of very small magnitude (Fig. 7*E*). Thus, our measurements show that the mechanisms that generate zero-spanning, but not offset, synchrony between nearby cells (within approximately 200 μm) show specificity to the orientation preference within the pair. For longer-range connections, both forms of synchrony show specificity for the orientation preference within the pair.

To fully characterize the structure of functional connectivity, we created a measure of connectivity strength by multiplying the probability of observing synchrony by the magnitude of the synchrony observed at each distance and $\Delta\theta$ (Fig. 7*C*,*F*). We call this metric functional connectivity "power". For zero-spanning synchrony, connection power showed a similar parametric dependence on distance and $\Delta\theta$ as probability and magnitude alone. That is, the strongest zero-spanning power was for nearby and similarly tuned cells, decreasing with both distance and $\Delta\theta$ (Fig. 7*C*).

The power of offset synchrony had a similar parametric dependence as the power of zero-spanning synchrony, again showing the strongest functional connectivity for nearby and similarly tuned cells, decreasing with both distance and $\Delta\theta$ (Fig. 7*F*). Unlike zero-spanning power, the structure of the power of offset synchrony was however created by the combination of complementary dependencies: the effect of $\Delta\theta$ at distances >500 μm was conferred by the probability (Fig. 7*D*), while the effect of $\Delta\theta$ at local distances was conferred by the magnitude (Fig. 7*E*). These plots demonstrate that functional connectivity can be organized in the absence of a functional architecture. In addition, the powers of functional connectivity of zero-spanning and offset synchrony show matching organization: highest for nearby cells with the similar orientation preference, lowest for distant pairs of the orthogonal orientation preference. Our data show functional connectivity that reflects the synaptic specificity of input to and within layer 2/3, in

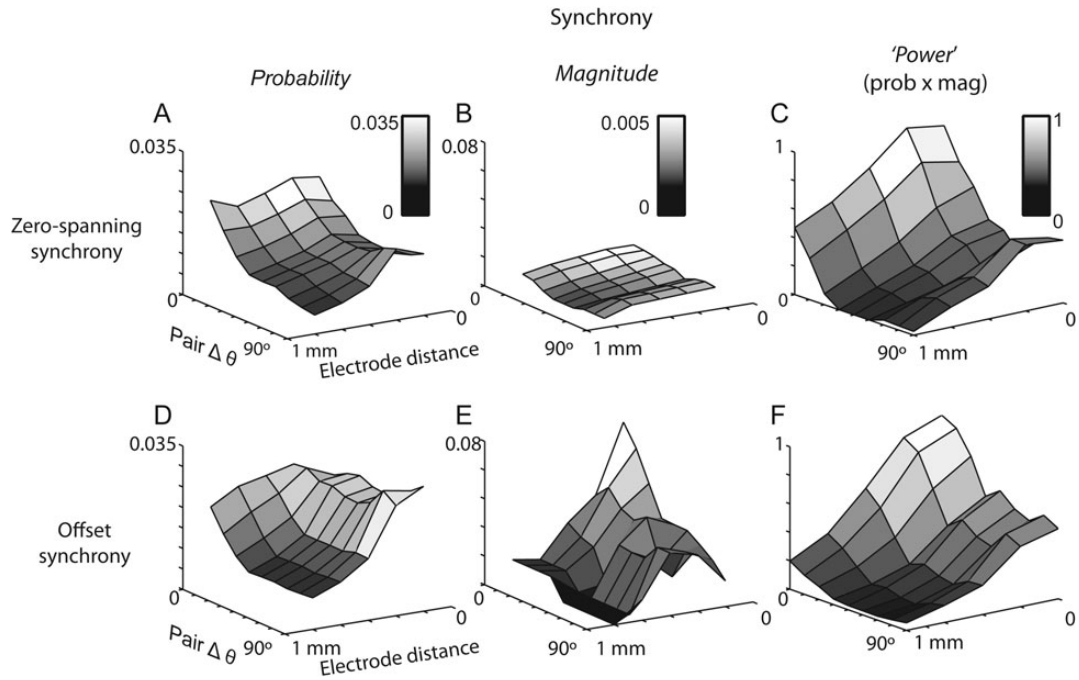

Figure 7. The structure of synchrony across distance and orientation preference. (*A–C*) Zero-spanning synchrony depends on distance and $\Delta\theta$. Probability (*A*), magnitude (*B*), and synchrony power (*C*) decayed exponentially from nearby, closely aligned pairs. (*D–F*) Offset synchrony depends on distance and $\Delta\theta$. The probability of direct synchrony (*D*) was independent of $\Delta\theta$ for nearby pairs, but dependent on $\Delta\theta$ at greater distances. Magnitude (*E*) was dependent on $\Delta\theta$ at all distances, and synchrony power (*F*) decayed exponentially from nearby, closely aligned pairs.

agreement with predictions based on in vitro measurements (Yoshimura and Callaway 2005; Ko et al. 2011).

Correlated Variability

The correlated fluctuation of trial-to-trial response magnitude, or correlated variability (r_{sc}), can have repercussions for how populations of neurons represent sensory responses from both the encoding and decoding perspectives (Johnson 1980; Zohary et al. 1994; Panzeri et al. 1999; Pouget et al. 2003; Averbeck and Lee 2006; Averbeck et al. 2006; Cohen and Kohn 2011). Under our conditions, we observed an evoked r_{sc} across our population of 0.16 ± 0.003 (mean ± SD; Fig. 8*A*, left, gray histogram, mean indicated by gray arrow). This value is similar to that measured in anesthetized macaque V1 over a comparable scale (Gawne and Richmond 1993; Reich et al. 2001; Kohn and Smith 2005; Smith and Kohn 2008) and cat V1 (Das and Gilbert 1999). We quantified a "spontaneous" r_{sc} using the periods between presentations of visual stimuli. To account for adaptation effects from the preceding stimulus, we calculated a spontaneous r_{sc} from periods subsequent to stimuli of the same orientation, and averaged across all orientations. Accounting for adaptation effects reduced spontaneous r_{sc} primarily for nearby pairs (data not shown). The r_{sc} calculated from epochs of spontaneous activity (0.15 ± 0.005; Fig. 8*A*, black histogram, mean indicated by black arrow) was not significantly higher than evoked r_{sc} ($P = 0.13$). Spontaneous r_{sc} was highly correlated with evoked r_{sc} (linear fit slope = 0.82 ± 0.02, $R^2 = 0.47$, Fig. 8*A*, right).

Correlated Variability as a Function of Distance and Orientation Preference

At our spatial scale, we observed a dependence of evoked r_{sc} on distance, well fit by an exponential decay function ($\chi^2 = 0.004$, $\tau = 209.9$ μm; Fig. 8*B*, left panel). It is important to note that although the area of cortex over which we measured correlation (approximately 1 mm) is more limited than in studies of other species, the span of visual space covered by our recordings is actually slightly larger (approximately 60° of visual space; Kalatsky and Stryker 2003). The decay in evoked r_{sc} with distance ($\tau = 209.9$ μm; Fig. 8*B*, left) was most similar to the decay in offset magnitude ($\tau = 162.9$ μm; Fig. 5*C*). The fit parameters used to fit the magnitude of offset synchrony fit the decay of evoked r_{sc} with $\chi^2 = 3 \times 10^{-4}$, consistent with a conclusion that trial-to-trial correlated variability is at least partially mediated by connectivity within L2/3.

We further investigated correlated variability by examining the relationship between $\Delta\theta$ and r_{sc}. In the presence of functional architecture, evoked r_{sc} depends on orientation tuning similarity (Smith and Kohn 2008). While we did observe an initial decay of evoked r_{sc} with increasing $\Delta\theta$, evoked r_{sc} increased at larger $\Delta\theta$ leading to a slightly *U*-shaped dependence (Fig. 8*C*, left). Still, this dependence was fit with an exponential decay ($\tau = 11.7°$, $\chi^2 = 2 \times 10^{-4}$).

Finally, we were able to measure the codependence of evoked r_{sc} on distance and $\Delta\theta$ (Fig. 8*D*, left), as we did for synchrony (Fig. 7). At short distances, evoked r_{sc} depended on $\Delta\theta$, while at distances >500 μm, r_{sc} was independent of $\Delta\theta$. The two-dimensional relationship of evoked r_{sc} closely matched that of synchrony power. We further explore the relationship between evoked r_{sc} and functional connectivity below (Fig. 10).

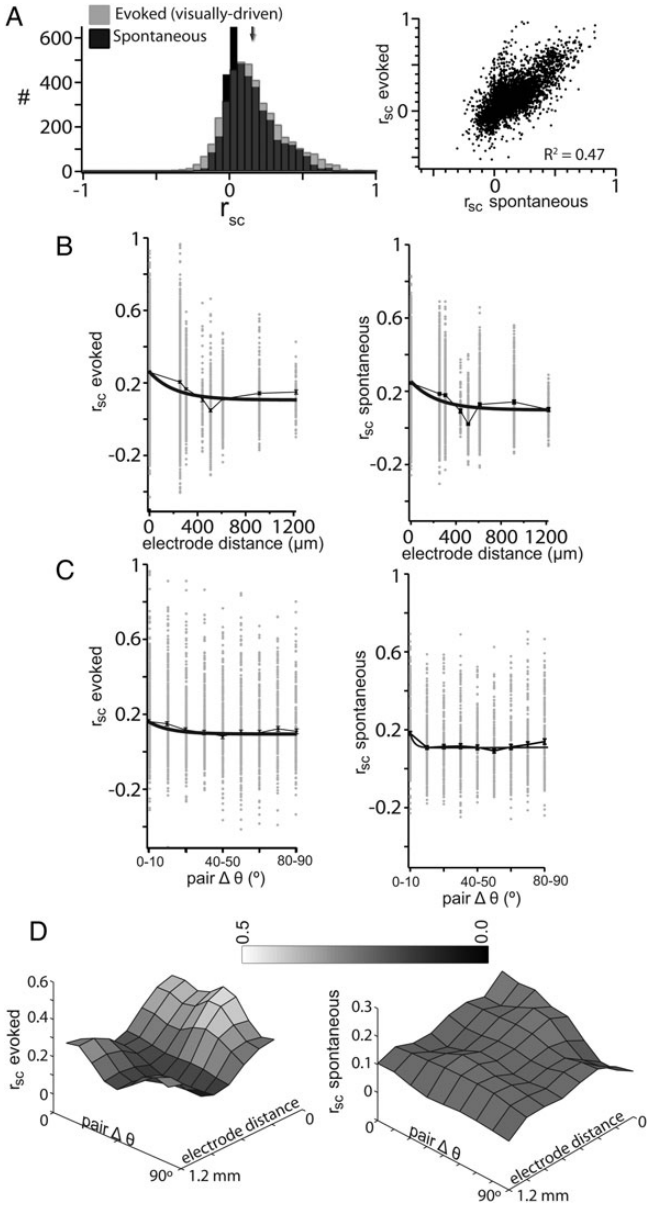

Figure 8. The structure of correlated variability across distance and orientation preference. (*A*) Distributions of evoked (gray) and spontaneous (black) r_{sc} were nonzero (left). Evoked r_{sc} was positively correlated with spontaneous r_{sc} (right). (*B*) Evoked and spontaneous, r_{sc}, decayed with distance between a pair of cells. (*C*) Evoked and spontaneous, r_{sc}, was dependent on the difference in orientation preference between a pair of cells. (*D*) Spontaneous and evoked, r_{sc}, have a stronger dependence on $\Delta\theta$ at smaller distances.

The structure of evoked r_{sc} demonstrates that correlation can be organized in the absence of functional architecture.

Correlated Variability of Spontaneous Activity

The correlated variability of spontaneous activity could have different spatial properties than that of evoked activity. Similar to evoked r_{sc}, we observed a dependence of spontaneous r_{sc} on the distance between the pair (Ch'Ng and Reid 2010) ($\tau = 235.3$ μm, $\chi^2 = 0.013$; Fig. 8*B*, right). $\Delta\theta$ had a weak effect on the measured spontaneous r_{sc} ($\tau = 3.0°$, $\chi^2 = 3 \times 10^{-4}$; Fig. 8*C*, right). A stronger dependence of spontaneous r_{sc} on $\Delta\theta$ was apparent for nearby pairs (Fig. 8*D*, right), as has been previously

observed in rodents (Ch'ng and Reid 2010). The relatively flat spatial and orientation tuning structure of spontaneous r_{sc} (Fig. 8*D*, right) suggests that the source of input responsible for these correlations operates nonspecifically over a distance >1 mm in mouse V1, distinct from the sources of synchrony.

Correlated Variability as a Function of Network State

It has been argued that the conditions that give rise to correlated variability of the magnitude observed here are not physiologically relevant (Ecker et al. 2010), namely that correlated variability is aberrantly increased by several factors, including clustering error and anesthetic-induced network state. To assess the role of network state on correlated variability, we quantified network synchronization using the spectral content of LFP recordings. The level of gamma activity either immediately preceding or during evoked activity did not affect the value of r_{sc} observed (Supplementary Fig. 3). To more directly assess the role of anesthesia on r_{sc}, we measured r_{sc} in awake, head-fixed mice under the same visual stimulus paradigm. Under these conditions, spontaneous and evoked firing rates were higher than under anesthesia (spontaneous mean: 2.8 ± 2.12 Hz; evoked mean: 8.082 ± 7.52 Hz; Fig. 9*A*), but cells showed similar orientation tuning (Fig. 9*B*). As such, these conditions eliminate two of the proposed confounding factors in measuring r_{sc}: anesthetic-induced synchronization and dampened firing rates. Despite this, evoked r_{sc} was very similar in the anesthetized and awake states (anesthetized: 0.16 ± 0.002, awake: 0.18 ± 0.03, $P = 0.34$; Fig. 9*C*). In contrast, spontaneous r_{sc} ($0.03 + 0.01$) was much lower in the awake state than that observed in the anesthetized state (anesthetized: 0.36 ± 0.004, $P < 0.01$; Fig. 9*C*), likely due to the lack of a slow oscillation in the LFP. In summary, measurements of correlation in the awake state were not different than those measured under our anesthetic regime.

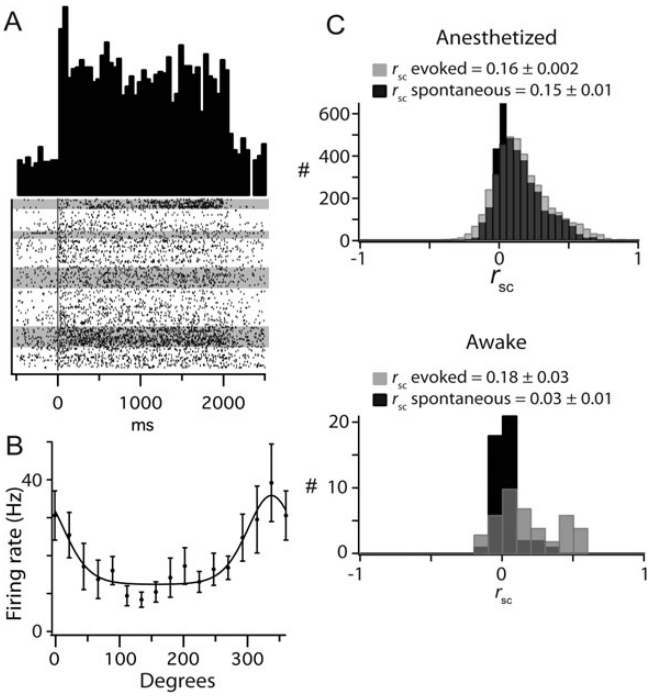

Figure 9. r_{sc} is not affected by anesthetic state. (*A*) PSTH and spike rasters from a single unit recorded from V1 of an awake, head-fixed mouse. Gray shading of spike rasters indicates epochs of locomotion. (*B*) Orientation tuning of cell in *A*. (*C*) The distributions of evoked r_{sc} were the same in anesthetized (top) and awake (bottom) states, while that of spontaneous r_{sc} were higher in the anesthetized (top) than awake (bottom) states.

The Relationship Between Correlated Variability and Synchrony

To investigate the origin of correlated variability, and to directly assess the relationship between the two timescales of correlation measured here, we sought to determine if correlated variability was predictive of either the probability or the magnitude of synchrony between pairs. To do this, we classified each of the 4160 pairs based on their value of evoked and spontaneous r_{sc}. We sorted each pair into one of three classes: High, moderate, or low r_{sc} according to the distribution of r_{sc} values (Fig. 10*A*). The thresholds for high (evoked $r_{sc} > 0.36$; spontaneous $r_{sc} > 0.31$; Fig. 10*A,B*, light gray) and low (evoked $r_{sc} < -0.04$; spontaneous $r_{sc} < -0.02$; Fig. 10*A,B*, black) classes were set one SD above and below the mean, respectively. The probability (Fig. 10*C*, left) and magnitude (right) of zero-spanning synchrony within each r_{sc} class were highest for pairs with high evoked r_{sc}. In contrast, the probability and magnitude of zero-spanning synchrony were highest for pairs close to the mean value of spontaneous r_{sc} (Fig. 10*C*, right), indicating a dissociation of the source of spontaneous r_{sc} from both evoked r_{sc} and zero-spanning synchrony. We observed even probability of offset synchrony across evoked r_{sc} classes, with higher CCG magnitude for pairs with midlevel r_{sc} (Fig. 10*D*), suggesting the mechanisms that generate offset synchrony have relatively less impact in determining the correlation of spike count variability.

Discussion

We measured the pairwise correlation of spike output in mouse V1 in response to visual stimulation on two timescales: synchronous spikes within ±10 ms and covariations in the mean evoked firing rate. Each has implications for information processing, depending on the neural implementation of decoding. We measured synchrony using pairwise CCGs and found that both the magnitude and probability of positive CCGs were a function of the difference in orientation tuning and distance between the two neurons in the pair, a functional structure despite the absence of columns.

We measured pairwise correlated variability (r_{sc}) of mean trial spike counts using Pearson's correlation coefficient. We found a small but significant value of r_{sc} (0.16 ± 0.01), similar to most of the studies in the literature. This magnitude was not due to anesthesia, as it was not significantly different in awake, actively moving mice. We found that r_{sc} depended on interneuronal distance and on the difference of orientation preference. Our results revealed a structure of neuronal correlations independent of a functional architecture.

Synchrony and Functional Connectivity

Cross-correlation techniques were originally developed to demonstrate functional connectivity between pairs of neurons (Perkel et al. 1967). We observed two types of positive CCG. The most common (234 of 4160 pairs; 5.6%) was a central peak straddling the zero line. We classified these as zero-spanning input because this shape could encompass

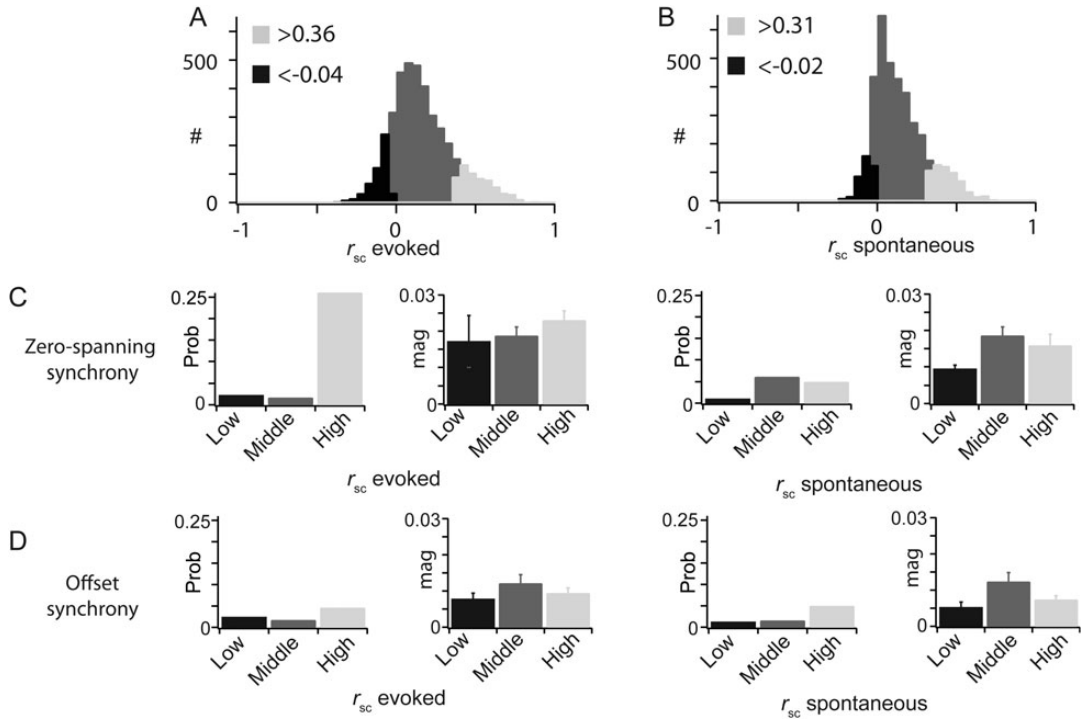

Figure 10. r_{sc} is correlated with zero spanning, but not offset synchrony. (*A* and *B*) Each pair was classified as high, mid, or low r_{sc}, for both evoked (*A*) and spontaneous (*B*) correlated variabilities, based on the total distribution of r_{sc} values (top). (*C*) Pairs with high evoked r_{sc} had a higher probability of having zero-spanning synchrony. Pairs with high evoked r_{sc} had a larger magnitude of zero-spanning synchrony. (*D*) Level of r_{sc}, either spontaneous or evoked, did not affect either the probability or magnitude of offset synchrony.

complex synaptic arrangements, including common excitatory input and direct connections. The second type of CCG (90 of 4160; 2.2%) showed the entire positive peak offset from the zero line by a few milliseconds, compatible with monosynaptic latency. While this shape is not sufficient to establish connectivity, which can only be demonstrated with dual simultaneous intracellular recordings (Thomson and Lamy 2007) or electron microscopy (Bock et al. 2011), we consider this evidence of a direct excitatory connection (Perkel et al. 1967; Ostojic et al. 2009).

At the short distances recorded by a single tetrode, the probability and magnitude of zero-spanning synchrony decreased as a function of relative orientation preference ($\Delta\theta$) (Fig. 7). As in columnar organization, L2/3 visual responses were dominated by orientation-specific L4 input, in agreement with specific connectivity between L4 and subnetworks of L2/3 pyramidal cells demonstrated in rodent visual cortex in vitro (Yoshimura and Callaway 2005). In contrast, the probability of offset synchrony at short distances was not dependent on $\Delta\theta$, consistent with diffuse L2/3 pyramidal cell axons in the local vicinity (Malach et al. 1993; Bosking et al. 1997; Van Hooser et al. 2006). As opposed to apparent local promiscuity, distant functional connectivity (>500 μm) was highly dependent on orientation tuning as in cat (Ts'o et al. 1986; Gilbert and Wiesel 1989; Bringuier et al. 1999), ferret (Tucker and Katz 2003), and macaque (Smith and Kohn 2008) V1. Our measurements suggest that common input is strongest within a 500-μm radius, matching the width of a receptive field, while strong offset synchrony spanned a shorter distance (Fig. 5*B*,*C*). Instances of offset synchrony that span longer distances linked excitatory cells with similar orientation preference over approximately 30° of visual space.

To provide a more complete picture of functional connectivity, we generated a metric that combines probability and magnitude, called connection "power." Like postsynaptic potentials (Ko et al. 2011), functional connectivity "power" depended on orientation and distance, for both zero-spanning and offset synchrony. Our results identify a functional role for specific synaptic connections: the organization of synchronous spike generation in local networks.

Observations of networks of synchronous cells are critical for large-scale models of V1 (McLaughlin et al. 2003; Seriès et al. 2004). Our observation of structured functional connectivity does not support models based on local random connectivity, either vertical or horizontal (Hansel and van Vreeswijk 2012).

Structure of r_{sc} and Synchrony

Columnar organization determines that nearby neurons share tuning properties and similar noise sources. As a result, there is significant correlation between tuning properties and trial-to-trial variability. In mouse V1, however, such arrangement is not trivial. Our data show that synchrony "power" decays exponentially along both the orientation and distance dimensions. We suggest that synaptic specificity within the apparent orientation domain disorganization preserves the structure of functional connectivity. Correlated variability is also weakly organized in the orientation domain (Fig. 8*C*); this structure may be partially inherited from contributions of functional connectivity (Fig. 10). Regardless of origin, our data indicate that the structures of correlated variability and synchrony represent an organizing principle of mammalian visual systems.

Along the distance domain, the decrement in synchrony in mouse V1 matched that in macaque V1 (Smith and Kohn 2008), when interneuronal distance is considered in terms of visual space. In mouse, correlation extended over less physical brain distance but more visual space, by a factor of 30 (30 vs. approximately 1°). This difference can be partially accounted for by the difference in receptive field diameter. As in macaque, synchrony in mouse V1 required some receptive field overlap, though less: we observed synchrony at all levels of overlap, whereas monkey required >50% overlap. Synchrony in cat V1 does not strictly require overlap (Ts'o et al. 1986), but it is dependent on the amount of overlap.

Spike Count Variability and Coding

Small pairwise correlations in variability limit the effectiveness of increasing the signal-to-noise ratio by pooling over many neurons (Zohary et al. 1994; Bair et al. 2001; Reich et al. 2001). Therefore, determining accurately the magnitude and structure of correlated variability is essential to constrain coding models based on pooled firing rates (Abbott and Dayan 1999). Although some estimate near-zero correlated variability in V1 (Ecker et al. 2010, but see Cohen and Kohn 2011), our results agree with a small, nonuniform level of evoked correlated variability independent of firing rate and anesthetic state (Fig. 9).

Correlated variability of spontaneous activity was weakly dependent on distance (Fig. 8), consistent with other studies in rodent V1 (Ch'Ng and Reid 2010). The weakness of correlation observed in rodents, together with the lack of correlation from macaque V1 (Smith and Kohn 2008), suggests a source of variability during spontaneous activity that is uniform over V1. Only at the local level (pairs separated by <500 μm) was spontaneous correlated variability organized by difference in preferred orientation, reflecting the preferred orientation specificity of synchrony (Fig. 7) and synaptic connections (Ko et al. 2011).

Our results showed a significant dependence of evoked correlated variability on distance and a weaker dependence on orientation preference. We suggest that the sources of evoked correlated variability are organized by the functional architecture. We were able to correlate high evoked correlated variability with the presence of zero-spanning synchrony, but not offset synchrony (Fig. 10), suggesting that correlated variability is partially mediated by shared sources of synaptic excitatory input, but not local excitatory connectivity.

Synchrony and Coding

Regardless of the underlying functional connectivity, synchronous spikes are critical for driving postsynaptic cells in noisy synaptic environments in vivo. Synchronized input more effectively drives a postsynaptic neuron than nonsynchronized increases in firing rate (Bruno and Sakmann 2006). Enhanced effectiveness of synchronized spikes derives from supralinear summation of short interspike interval post-synaptic potentials (PSPs). In L4 of cat V1 in vivo, supralinear summation of visually evoked excitatoty PSPs depends on the delay between excitation and inhibition within a window of 0–20 ms (Cardin et al. 2010); elsewhere in sensory systems, sensitivity to coincidence requires intervals of <10 ms (Alonso et al. 1996; Roy and Alloway 2001; Kumbhani et al. 2007). Supralinear summation in vitro depends on Na^+ and Ca^{2+} dendritic conductances with a 0- to 30-ms effective summation interval (Nettleton and Spain 2000) and can overcome the strong synaptic depression in cortical cells (Bannister and Thomson 2006). Given firing rates of mouse V1 cells to artificial stimuli (<10 Hz), and other visual systems to natural stimuli (Vinje and Gallant 2000; Haider et al. 2010), summation within these intervals requires heterosynaptic summation through synchrony.

It has been proposed that representation of information in neuronal networks depends on synchrony. While pairwise analysis in the retina adds <10% to the information that can be extracted from independent responses (Nirenberg et al. 2001; Schneidman et al. 2003), higher-order correlations increase information by as much as 20% (Pillow et al. 2008). In the lateral geniculate nucleus, up to 20% additional information can be extracted from pairwise correlations (Dan et al. 1998). In V1, synchrony between pairs of cells can be used to better discriminate gratings with fine, but not course, orientation differences (Samonds et al. 2003, 2004), supporting a role for synchrony. It is not known if correlated spikes in the millisecond timescale are used by the brain to decode population activity, but these, and theoretical results (reviewed in Harris 2005), underscore the need for simultaneous recordings of multiple neurons and the identification of higher statistical dependencies (Nirenberg and Latham 2003; Schneidman et al. 2006; Pillow et al. 2008).

Our data show that about 8% of neuronal pairs fired synchronous spikes within a window of ±10 ms. This synchrony depends on distance and orientation preference. Because of stimulus limitations, clustering resolution, and low spike rates, our measurements represent a lower bound on the amount of synchrony among cortical cells and reinforce the notion that, to understand neural coding, neuronal responses should not be treated independently.

Supplementary Material

Supplementary material can be found at: http://www.cercor.oxfordjournals.org/.

Funding

This work was supported by the National Eye Institute (NIH R01 EY020765 and the University of Pennsylvania Vision Training Grant 2T32EY00735).

Notes

The authors acknowledge Larry Palmer for assistance with visual stimuli, Jason Wester, Morgan Taylor, and Amy Campbell for reading versions of this manuscript, and all members of the Contreras lab for helpful discussion. *Conflict of Interest*: None declared.

References

Abbott LF, Dayan P. 1999. The effect of correlated variability on the accuracy of a population code. Neural Comput. 11:91–101.

Alonso JM, Usrey WM, Reid RC. 1996. Precisely correlated firing in cells of the lateral geniculate nucleus. Nature. 383:815–819.

Averbeck BB, Latham PE, Pouget A. 2006. Neural correlations, population coding and computation. Nat Rev Neurosci. 7:358–366.

Averbeck BB, Lee D. 2006. Effects of noise correlations on information encoding and decoding. J Neurophysiol. 95:3633–3644.

Bair W, Zohary E, Newsome WT. 2001. Correlated firing in macaque visual area MT: time scales and relationship to behavior. J Neurosci. 21:1676–1697.
Bannister AP, Thomson AM. 2006. Dynamic properties of excitatory synaptic connections involving layer 4 pyramidal cells in adult rat and cat neocortex. Cereb Cortex. 17:2190–2203.
Bock DD, Lee W-CA, Kerlin AM, Andermann ML, Hood G, Wetzel AW, Yurgenson S, Soucy ER, Kim HS, Reid RC. 2011. Network anatomy and in vivo physiology of visual cortical neurons. Nature. 471:177–182.
Bonin V, Histed MH, Yurgenson S, Reid RC. 2011. Local diversity and fine-scale organization of receptive fields in mouse visual cortex. J Neurosci. 31:18506–18521.
Bosking WH, Zhang Y, Schofield B, Fitzpatrick D. 1997. Orientation selectivity and the arrangement of horizontal connections in tree shrew striate cortex. J Neurosci. 17:2112–2127.
Bringuier V, Chavane F, Glaeser L, Frégnac Y. 1999. Horizontal propagation of visual activity in the synaptic integration field of area 17 neurons. Science. 283:695–699.
Bruno RM, Sakmann B. 2006. Cortex is driven by weak but synchronously active thalamocortical synapses. Science. 312:1622–1627.
Buzsáki G, Anastassiou CA, Koch C. 2012. The origin of extracellular fields and currents—EEG, ECoG, LFP and spikes. Nat Rev Neurosci. 13:407–420.
Cardin JA, Kumbhani RD, Contreras D, Palmer LA. 2010. Cellular mechanisms of temporal sensitivity in visual cortex neurons. J Neurosci. 30:3652–3662.
Ch'ng YH, Reid RC. 2010. Cellular imaging of visual cortex reveals the spatial and functional organization of spontaneous activity. Front Integr Neurosci. 4:1–9.
Cohen MR, Kohn A. 2011. Measuring and interpreting neuronal correlations. Nat Neurosci. 14:811–819.
Dan Y, Alonso JM, Usrey WM, Reid RC. 1998. Coding of visual information by precisely correlated spikes in the lateral geniculate nucleus. Nat Neurosci. 1:501–507.
Das A, Gilbert CD. 1999. Topography of contextual modulations mediated by short-range interactions in primary visual cortex. Nature. 399:655–661.
de la Rocha J, Doiron B, Shea-Brown E, Josić K, Reyes A. 2007. Correlation between neural spike trains increases with firing rate. Nature. 448:802–806.
Deneve S, Latham P, Pouget A. 1999. Reading population codes: a neural implementation of ideal observers. Nat Neurosci. 2:740–745.
Ecker AS, Berens P, Keliris GA, Bethge M, Logothetis NK, Tolias AS. 2010. Decorrelated neuronal firing in cortical microcircuits. Science. 327:584–587.
Gao E, DeAngelis GC, Burkhalter A. 2010. Parallel input channels to mouse primary visual cortex. J Neurosci. 30:5912–5926.
Gawne TJ, Richmond BJ. 1993. How independent are the messages carried by adjacent inferior temporal cortical neurons? J Neurosci. 13:2758–2771.
Gawne TJ, Richmond BJ, Optican LM. 1991. Interactive effects among several stimulus parameters on the responses of striate cortical complex cells. J Neurophysiol. 66:379.
Gilbert CD, Wiesel TN. 1989. Columnar specificity of intrinsic horizontal and corticocortical connections in cat visual cortex. J Neurosci. 9:2432–2442.
Haider B, Krause MR, Duque A, Yu Y, Touryan J, Mazer JA, McCormick DA. 2010. Synaptic and network mechanisms of sparse and reliable visual cortical activity during nonclassical receptive field stimulation. Neuron. 65:107–121.
Hansel D, van Vreeswijk C. 2012. The mechanism of orientation selectivity in primary visual cortex without a functional map. J Neurosci. 32:4049–4064.
Harris KD. 2005. Neural signatures of cell assembly organization. Nat Rev Neurosci. 6:399–407.
Harrison MT, Geman S. 2009. A rate and history-preserving resampling algorithm for neural spike trains. Neural Comput. 21:1244–1258.
Hofer SB, Ko H, Pichler B, Vogelstein J, Ros H, Zeng H, Lein E, Lesica NA, Mrsic-Flogel TD. 2011. Differential connectivity and response dynamics of excitatory and inhibitory neurons in visual cortex. Nat Neurosci. 14:1045–1052.
Jia H, Rochefort NL, Chen X, Konnerth A. 2010. Dendritic organization of sensory input to cortical neurons *in vivo*. Nature. 464:1307–1312.
Johnson KO. 1980. Sensory discrimination: neural processes preceding discrimination decision. J Neurophysiol. 43:1793–1815.
Kalatsky VA, Stryker MP. 2003. New paradigm for optical imaging: temporally encoded maps of intrinsic signal. Neuron. 38:529–545.
Ko H, Hofer SB, Pichler B, Buchanan KA, Sjöström PJ, Mrsic-Flogel TD. 2011. Functional specificity of local synaptic connections in neocortical networks. Nature. 473:87–91.
Kohn A, Smith MA. 2005. Stimulus dependence of neuronal correlation in primary visual cortex of the macaque. J Neurosci. 25:3661–3673.
Kruger J, Aiple F. 1988. Multimicroelectrode investigation of monkey striate cortex: spike train correlations in the infragranular layers. J Neurophysiol. 60:798.
Kumbhani RD, Nolt MJ, Palmer LA. 2007. Precision, reliability, and information-theoretic analysis of visual thalamocortical neurons. J Neurophysiol. 98:2647–2663.
Malach R, Amir Y, Harel M, Grinvald A. 1993. Relationship between intrinsic connections and functional architecture revealed by optical imaging and in vivo targeted biocytin injections in primate striate cortex. Proc Natl Acad Sci. 90:10469–10473.
McLaughlin D, Shapley R, Shelley M. 2003. Large-scale modeling of the primary visual cortex: influence of cortical architecture upon neuronal response. J Physiol Paris. 97:237–252.
Nettleton JS, Spain WJ. 2000. Linear to supralinear summation of AMPA-mediated EPSPs in neocortical pyramidal neurons. J Neurophysiol. 83:3310–3322.
Niell CM, Stryker MP. 2008. Highly selective receptive fields in mouse visual cortex. J Neurosci. 28:7520–7536.
Niell CM, Stryker MP. 2010. Modulation of visual responses by behavioral state in mouse visual cortex. Neuron. 65:472–479.
Nirenberg S, Carcieri SM, Jacobs AL, Latham PE. 2001. Retinal ganglion cells act largely as independent encoders. Nature. 411:698–701.
Nirenberg S, Latham PE. 2003. Decoding neuronal spike trains: how important are correlations? Proc Natl Acad Sci. 100:7348–7353.
Ohki K, Chung S, Ch'ng YH, Kara P, Reid RC. 2005. Functional imaging with cellular resolution reveals precise micro-architecture in visual cortex. Nature. 433:597–603.
Ostojic S, Brunel N, Hakim V. 2009. How connectivity, background activity, and synaptic properties shape the cross-correlation between spike trains. J Neurosci. 29:10234–10253.
Panzeri S, Schultz SR, Treves A, Rolls ET. 1999. Correlations and the encoding of information in the nervous system. Proc Roy Soc B Biol Sci. 266:1001–1012.
Perkel DH, Gerstein GL, Moore GP. 1967. Neuronal spike trains and stochastic point processes. Biophys J. 7:391–418.
Pillow JW, Shlens J, Paninski L, Sher A, Litke AM, Chichilnisky EJ, Simoncelli EP. 2008. Spatio-temporal correlations and visual signalling in a complete neuronal population. Nature. 454:995–999.
Pouget A, Dayan P, Zemel RS. 2003. Inference and computation with population codes. Ann Rev Neurosci. 26:381–410.
Pouget A, Deneve S, Ducom JC, Latham PE. 1999. Narrow versus wide tuning curves: what's best for a population code? Neural Comput. 11:85–90.
Reich DS, Mechler F, Victor JD. 2001. Independent and redundant information in nearby cortical neurons. Science. 294:2566–2568.
Reid RC, Alonso JM. 1996. The processing and encoding of information in the visual cortex. Curr Opin Neurobiol. 6:475–480.
Romo R, Hernández A, Zainos A, Salinas E. 2003. Correlated neuronal discharges that increase coding efficiency during perceptual discrimination. Neuron. 38:649–657.
Roy SA, Alloway KD. 2001. Coincidence detection or temporal integration? What the neurons in somatosensory cortex are doing. J Neurosci. 21:2462–2473.
Samonds JM, Allison JD, Brown HA, Bonds AB. 2003. Cooperation between area 17 neuron pairs enhances fine discrimination of orientation. J Neurosci. 23:2416–2425.

Samonds JM, Allison JD, Brown HA, Bonds AB. 2004. Cooperative synchronized assemblies enhance orientation discrimination. Proc Natl Acad Sci. 101:6722–6727.
Schmitzer-Torbert N, Jackson J, Henze D, Harris K, Redish AD. 2005. Quantitative measures of cluster quality for use in extracellular recordings. Neuroscience. 131:1–11.
Schneidman E, Berry MJ, Segev R, Bialek W. 2006. Weak pairwise correlations imply strongly correlated network states in a neural population. Nature. 440:1007–1012.
Schneidman E, Still S, Berry MJ, Bialek W. 2003. Network information and connected correlations. Phys Rev Lett. 91(238701):1–4.
Seriès P, Latham PE, Pouget A. 2004. Tuning curve sharpening for orientation selectivity: coding efficiency and the impact of correlations. Nat Neurosci. 7:1129–1135.
Smith MA, Kohn A. 2008. Spatial and temporal scales of neuronal correlation in primary visual cortex. J Neurosci. 28:12591–12603.
Swindale NV. 1998. Orientation tuning curves: empirical description and estimation of parameters. Biol Cybern. 78:45–56.
Thomson AM, Lamy C. 2007. Functional maps of neocortical local circuitry. Front Neurosci. 1:19–42.
Ts'o DY, Gilbert CD, Wiesel TN. 1986. Relationships between horizontal interactions and functional architecture in cat striate cortex as revealed by cross-correlation analysis. J Neurosci. 6:1160–1170.
Tucker TR, Katz LC. 2003. Spatiotemporal patterns of excitation and inhibition evoked by the horizontal network in layer 2/3 of ferret visual cortex. J Neurophysiol. 89:488–500.
Van Hooser SD, Heimel JA, Chung S, Nelson SB. 2006. Lack of patchy horizontal connectivity in primary visual cortex of a mammal without orientation maps. J Neurosci. 26:7680–7692.
Vinje WE, Gallant JL. 2000. Sparse coding and decorrelation in primary visual cortex during natural vision. Science. 287:1273–1276.
Yoshimura Y, Callaway EM. 2005. Fine-scale specificity of cortical networks depends on inhibitory cell type and connectivity. Nat Neurosci. 8:1552–1559.
Yoshimura Y, Dantzker JLM, Callaway EM. 2005. Excitatory cortical neurons form fine-scale functional networks. Nature. 433:865–868.
Zohary E, Shadlen MN, Newsome WT. 1994. Correlated neuronal discharge rate and its implications for psychophysical performance. Nature. 370:140–143.